Optimal degeneracy for the signal recycling cavity in advanced LIGO

Yi Pan[1]

[1] *Theoretical Astrophysics and Relativity, California Institute of Technology, Pasadena, CA 91125*

(Dated: January 9, 2006)

As currently designed, the signal recycling cavity (SRC) in the Advanced LIGO interferometer is degenerate. In such a degenerate cavity, the phase fronts of optical fields become badly distorted when the mirror shapes are slightly deformed due to mirror figure error and/or thermal aberration, and this causes significant loss of the signal power and the signal-to-noise ratio (SNR) of a gravitational wave event. Through a numerical modal simulation of the optical fields in a simplified model of the Advanced LIGO interferometer, I investigate the SNR loss and the behavior of both the carrier and signal optical fields, with the SRC at various levels of degeneracy. I show that the SNR loss is severe with a degenerate SRC, and a non-degenerate SRC can be used to solve this problem. I identify the optimal level of degeneracy for the SRC, which is achieved with the cavity Gouy phase between 0.4 and 0.7 radian. I also discuss possible alternative designs of the SRC to achieve this optimal degeneracy.

PACS numbers:

I. INTRODUCTION

In Advanced LIGO [1], among other upgrades from initial LIGO [2], a signal recycling mirror (SRM) is introduced at the dark port output of the interferometer (see Fig. 1).

The SRM forms the signal recycling cavity (SRC) with the input test masses (ITMs); and the SRC and the arm cavity (AC) form a coupled resonant cavity, whose resonant properties can be controlled by two parameters of the SRM (position and reflectivity) [3, 4]. In Advanced LIGO, with much higher optical power in the AC (830kW), the SRM parameters are chosen to reduce the optical power in the recycling cavities that passes through the beamsplitter (BS), thus reducing the thermal distortions due to thermal lensing. This flexibility also enables the interferometer, although not in the Advanced LIGO baseline design, to change its frequency response between broad-band and narrow-band configurations, thus improving the detection of GW sources with specific frequency characteristics [7]. The Advanced LIGO baseline design has the interferometer working in the broadband resonant sideband extraction (RSE) configuration [4–6]. The signal recycling configuration, in principle, is also able to circumvent the fundamental quantum limit on measurement and go below the so called standard quantum limit (SQL).

Given the advantages and new physics the signal recycling configuration brings, however, there might be problems in the current design of the SRC.

The SRC, as well as the power recycling cavity (PRC), are near degenerate, and it is well known that degenerate cavities are not selective to optical modes and perturbations to the cavity geometry cause strong mode coupling[8]. Specifically, in the LIGO and Advanced LIGO interferometers, figure error and thermal aberration of the mirrors (PRM, SRM and ITMs) will cause strong optical mode coupling which transfers laser power from the fundamental mode to higher order modes

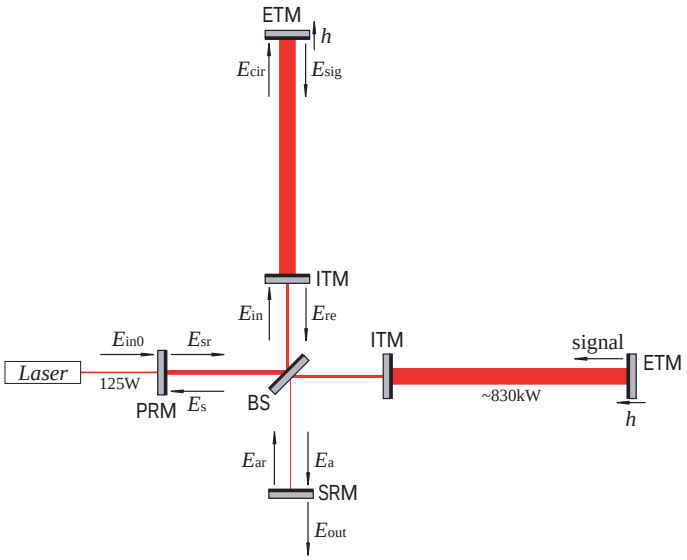

FIG. 1: Diagram of Advanced LIGO interferometer. A signal recycling mirror is placed at the dark port, forming a SR cavity with the ITMs.

(HOMs) and harm both the radio frequency (RF) sideband (in the PRC) and the signal sideband (in the SRC).

The consequence of the high PRC degeneracy is well known since severe mode mixing of the RF sideband has been observed in LIGO, and it did harm the control signal and affect the interferometer operation. Measures has been taken to fix the problem, including introducing the thermal compensation system (TCS) to reduce the thermal aberration on the mirror [9], and replacing bad optical elements with unexpected high absorption. However, there is still the worry about the Advanced LIGO, where much higher optical power in the AC will cause worse thermal aberration on the ITMs. Müller *et al* have been suggesting to reduce the PRC degeneracy by moving the mode-matching telescope (MMT) into the recy-

cling cavities to reduce the beam waist size [10] and they are currently working on practical issues in implementing this modified topology in AdvLIGO [11].

The consequence of the high SRC degeneracy is not yet clearly understood though since signal sideband behaves differently from the carrier or the RF sideband in the sense that it is resonant in the coupled two-cavity system formed by the AC and the SRC, unlike the carrier or the RF sideband which, roughly speaking, is resonant only in the non-degenerate AC or the degenerate PRC. The mode mixing of the signal sideband is seemingly somewhere between the carrier and the RF sideband.

Thorne [12] estimated the severeness of mode mixing in the signal sideband under the assumption that the light propagation in the SRC is well described by geometric optics (since degenerate cavity accommodates optical eigenmodes to very high orders, "light rays" with sharp edges are eigenmodes of the cavity as well), and found that for the signal to noise ratio (SNR) to reduce by less than 1% (assuming shot noise dominating) due to mode mixing, the *peak-to-valley* mirror figure error in the central region (region enclosing 95% of the ligh power) in the SRC has to be less than 2nm for a wideband AdvLIGO baseline design, and less than 1nm for narrowband configuration, independent of whether Gaussian beam or Mesa beam [12] is used, since degenerate cavity doesn't distinguish optical modes. These are severe constraints with current technology. More careful investigation of this problem and the alternative designs of low degeneracy SRC is needed.

In this paper, we present a mode decomposition based simulation of light propagation, including both the carrier and signal sideband, in a simplified Advanced LIGO interferometer model, and study the SNR loss due to mirror perturbations. We get similar constraints on the mirror figure error as in Ref. [12]. We also compute the optimal degeneracy of the SRC, at which the SNR loss due to mirror perturbations is minimized, assuming an ideal lens is added into the SRC to reduce the degeneracy. Consequently, we found that it is not practical to use a single lens to change the SRC degeneracy as the beam has to be focus so strongly to achieve the optimal degeneracy that the beam size on the SRM is on the order of 10^{-4}m, and the power density on it exceeds $10\mathrm{GW/m}^2$. We apply the MMT design Müller suggested for the PRC [10], which in principle, works also for the SRC. In this design, the beam size is brought down to millimeter scale by two mirrors to achieve the optimal degeneracy.

This paper is organized as follows. In Sec. II, we give a brief overview of the mode decomposition formalism and the Hermite-Gaussian modes [13], and interpret the cavity degeneracy in the modal space point of view. In Sec. III, we describe in detail the AdvLIGO interferometer model that is used in the simulation. In Sec. IV, we summarize the numerical result came out of the simulation, including the constraint on mirror figure error and thermal aberration and the optimal SRC degeneracy. We also investigated the requirement for the three alternative designs to achieve the optimal SRC degeneracy. At the end, we discuss the robustness of our simulation and possible improvement undergoing. In Sec. V, we summarize our conclusions.

II. MODE DECOMPOSITION FORMALISM

A. Modal decomposition in general

The mode decomposition formalism of calculating optical fields in a perturbed interferometer is demonstrated in detail by Hefetz *et al* [14]. We will review the general idea briefly in this section.

One can generally expand the electromagnetic (EM) field of a light beam as a superposition of orthonormal optical modes:

$$E(x,y,z) = \sum_n a_n U_n(x,y,z) \tag{1}$$

Though the basis modes $U_n(x,y,z)$ are arbitrary in principle, one choose preferably the eigenmodes of the cavities in the ideal interferometer, e.g. (i) Hermite-Gaussian modes, which are eigenmodes in the AdvLIGO baseline design cavities formed by spherical mirrors (assuming infinite mirror size); (ii) Mesa beam modes [12], which are eigenmodes suggested for AdvLIGO to reduce thermal noise. The complex vector space formed by $U_n(x,y,z)$ is call the *modal space*, and the EM field in modal space is represented by an complex vector a_n. The propagation of the optical field can thus be described by matrix in this modal space. In a Cartesian coordinate where the z-axis is along the optical axis and x and y-axes are transverse to it, an operator $M(x,y,z_2,z_1)$ transforms the EM field at position z_1 to the field at position z_2:

$$E(x,y,z_2) = M(x,y,z_2,z_1) \otimes E(x,y,z) \tag{2}$$

and the representation of $M(x,y,z_2,z_1)$ in the modal space is given by

$$M_{mn}(z_2,z_1) = \int\int_{-\infty}^{\infty} U_m^{\dagger}(x,y,z_2) M(x,y,z_2,z_1) U_n(x,y,z_1) dxdy \tag{3}$$

It is convenient to separate these operators into propagation operators in free space and interaction operators describing the EM fields transformation when interacting with optical elements. The free space propagator is given by:

$$P_{mn}(z_1,z_2) = \delta_{mn} e^{-ik(z_2-z_1)} e^{i\eta_n} \tag{4}$$

where k is the wave vector and η_n is the diffraction phase (i.e. the extra phase accumulated during propagation besides $k(z_2-z_1)$, due to diffraction effect, e.g. the Guoy phase of Gaussian beam) associated with the nth optical mode.

To write out the interaction operator, we choose, near the surfaces of an optical element, reference surfaces which match the phase front shapes of the ideal light beams. The operators can then be written in the general form

$$M_{mn} = \langle m|M(x,y)|n\rangle = \langle m|e^{-ikZ(x,y)}|n\rangle \qquad (5)$$

where $Z(x,y)$ is the optical path light travels from entering a reference surface into the optical element till leaving some reference surface. For ideal optical elements in our interferometer model, $Z(x,y) =$ constant, i.e. the mirrors or lens match exactly the optical modes and there is no coupling between optical modes when light beam interacts with the optical elements. For perturbed elements, e.g. slightly tilted mirrors, and slightly deformed mirrors due to figure error and/or thermal aberration, the optical modes couple to each other. $Z(x,y)$ contains contribution from both the figure error and the change of refraction index in the material, and is referred to as distortion function. $Z(x,y)$ can be complex, when used to describe lossy optical elements. These interaction operators need to be accompanied by the scalar reflectivity and transmissivity coefficients of the unperturbed optical element to give the true transform of the fields during interacting with the elements.

In writing the interaction operators, we adopted the short distance approximation [15], where the propagation inside optical element between the reference planes are approximated by a simple non-uniform phase factor. The phase distortion introduced by this approximation, besides a factor of the order unity determined by the geometry of the ideal cavity, is obtained in Ref. [15]

$$\Delta\Phi \sim \frac{1}{4\pi}\frac{\lambda}{L} \qquad (6)$$

where λ is the wavelength of the light and L is the length of the cavity. In LIGO or AdvLIGO, L is at least of the order 10 meters, and the phase distortion is thus smaller than 10^{-8}. Since a 1nm mirror figure error gives a phase distortion of 6×10^{-4}, $\Delta\Phi$ is always safely negligible.

In the modal space, the optical fields in a perturbed interferometer can be calculated from the unperturbed fields using linear algebra only, without solving the wave equations.

B. Hermite-Gaussian modes

In this section, we review briefly the Hermite-Gaussian modes [13] that is used as basis modes in our simulation.

A Hermite-Gaussian mode of beam waist size w_0 is given by [13]:

$$\begin{aligned} U_n(x,z) &= \left(\frac{2}{\pi}\right)^{1/4}\left(\frac{1}{2^n n! w(z)}\right)^{1/2} H_n\left(\frac{\sqrt{2}x}{w(z)}\right) \\ &\times\exp\left(-x^2\left(\frac{1}{w(z)^2}+\frac{ik}{2R(z)}\right)\right) \\ &\times\exp\left(i\left(m+\frac{1}{2}\right)\eta(z)\right) \end{aligned} \qquad (7)$$

where $H_n(x)$ is the Hermite polynomial and $R(z)$, $w(z)$ and $\eta(z)$ are the curvature radius of the phase front, the beam spot size and the Guoy phase respectively, given in terms of the Rayleigh length $z_0 = \pi w_0^2/\lambda$ by

$$\begin{aligned} R(z) = z + \frac{z_0^2}{z}, \qquad w(z) = w_0\sqrt{1+\frac{z^2}{z_0^2}} \\ \text{and} \qquad \eta(z) = \tan^{-1}\left(\frac{z}{z_0}\right) \end{aligned} \qquad (8)$$

These Hermite-Gaussian modes are exact solutions to the paraxial wave equation in one dimension, and they form an complete orthogonal basis in the space. We use Hermite-Gaussian modes as basis modes in the modal space:

$$E(x,y,z) = \sum_{mn} a_{mn}U_m(x,z)U_n(y,z)\exp(-ikz) \qquad (9)$$

where each transverse mode is labeled by two integers (m,n) corresponding to x and y dimensions.

The propagation operators are given in Eq. (4), with the diffraction phases replaced by the Gouy phases of the (m,n) Hermite-Gaussian modes: $(m+n+1)\eta(z)$. The interaction operators defined in Eq. (5) are derived analytically for Hermite-Gaussian modes in Ref. [14], assuming that the mirror radius is much larger than the beam size. This assumption is not valid everywhere in the LIGO or AdvLIGO interferometer, but we will not consider the correction caused by the diffraction loss (i.e. mode coupling due to finite mirror aperture) in this work.

Gaussian beams have spherical phase fronts, and are thus supported by cavities formed by spherical mirrors as eigenmodes. There are simple relations between the geometry of the cavity (measured by, e.g. cavity g-factor, mirror radius of curvature) and the physical properties of the Gaussian eigenmodes (e.g. beam waist size, waist position) that are available in Ref. [13].

To conclude this section, we use the baseline designs of the AC and the PRC in the AdvLIGO as examples to demonstrate quantitatively the degeneracy of cavities that . The curvature radii of the PR mirror and the test masses are

$$\begin{aligned} &R_{\rm ETM} = R_{\rm ITM} = 2076.4m \qquad R_{\rm ITM2} = -1186.4m \\ &R_{\rm PR} = 1194.7m \end{aligned} \qquad (10)$$

where RITM and RITM2 are curvature radii of the ITM seen from inside the AC and the PRC, respectively, and

the ITM is convex seen from the PRC. The cavity lengths are $d_{\rm AC} = 4000m$ and $d_{\rm PRC} = 8.34m$ and we have the Rayleigh lengths and Guoy phases

$$z_{0\,\rm AC} = 390.9m \qquad \eta_{\rm AC} = 0.39 \tag{11}$$

$$z_{0\,\rm PRC} = 82.1m \qquad \eta_{\rm PRC} = 4.9 \times 10^{-4} \tag{12}$$

In the AC, the Rayleigh length is clearly much shorter than the typical distance carrier light travels in the cavity, i.e. the light propagation is in the strong diffraction zone which indicates a non-degenerate cavity. More rigorously, the Guoy phase, corresponding to a frequency shift of

$$\Delta\nu = \frac{c}{2\pi d_{\rm AC}}\eta_{\rm AC} = 4.6kHz \tag{13}$$

which is much larger than the bandwidth of the AC ($\sim 15Hz$). This means, the Guoy phase breaks the degeneracy between the Gaussian modes with different orders (different $m+n$), i.e. when the cavity is tuned to have the fundamental mode in resonance, all other HOMs are suppressed.

In the PRC, the Rayleigh length is longer than the length of the cavity, but shorter than the typical distance RF sideband light travels inside the cavity after we count in the number of round trips (~ 50). So the RF sideband propagation in the PRC is still in its strong diffraction zone. Nevertheless, when we look at the Guoy phase, corresponding to a frequency shift of $\Delta\nu = 2.8kHz$, which is much smaller than the bandwidth of the PRC ($\sim 100kHz$). The PRC, although not degenerate to the extreme level that geometric optics becomes valid, accommodates tens of HOMs together with the fundamental mode, and is thus highly degenerate.

III. ADVANCED LIGO INTERFEROMETER MODELING

In this section, we describe our simplified model of the AdvLIGO interferometer, and the way our simulation works.

In our simulation, we study a AdvLIGO interferometer in equilibrium with static optical fields built inside it. We use the standard AdvLIGO optical topology displayed in Fig. 1, and the input light is a pure (0,0) Hermite-Gaussian mode coming in from the PR mirror. We consider both a broadband and a narrowband interferometer designs. The interferometer parameters for the broadband detector are chosen as their values in the AdvLIGO baseline design. The parameters in the two designs are listed below, where we started to use the following subscripts to denote different mirrors and cavities throughout the whole paper: "bs", "i", "e", "p" and "s" stand for the beam splitter (BS), ITM, ETM, PRM and SRM; "ac", "prc" and "src" stand for AC, PRC and SRC

(i) Cavity macroscopic length: The ACs both have $L = 4000m$; The common lengths of the PRC and the SRC are $l_{pc} = 8.34m$ and $l_{pc} = 8.327m$;

(ii) Cavity microscopic tuning: The carrier light gets the following amount of phase shift during a single trip in the AC, PRC and SRC

$$\phi_{ac} = \phi_{pc} = 0 \qquad \phi^{\rm B}_{\rm src} = 0.06 \qquad \phi^{\rm N}_{\rm src} = \pi - 1.556 \tag{14}$$

where the superscripts on the SRC phasing denote broadband (B) and narrowband (N). An asymmetry in the Micheleson arm lengths is introduced because, among other reasons, we choose the homodyne readout scheme where a tiny amount of the carrier light power goes toward the darkport and beat with the resonant signal sideband to give the detector output. For this purpose solely, the asymmetry here is specified at the microscopic level as the phase difference the carrier accumulates in the two Micheleson arms: $\Delta\phi = 0.01$.

(iii) Mirror power transmissivity:

$$t_i^2 = 0.5\% \qquad t_e^2 = 76\,\rm ppm \qquad t_p^2 = 5.9\%$$

$$t_s^{\rm B\,2} = 7\% \qquad t_s^{\rm N\,2} = 0.3\% \tag{15}$$

We assume lossless mirrors throughout our simulation, so the amplitude reflectivity and transmissivity are completely determined.

(iv) Mirror curvature radius: Given in Eq. (10) except for the SRM. We introduce a lens between the beamsplitter and the SRM to change the beam shape and degeneracy in the SRC, so the curvature radius of the SRM, thus also the cavity g-factor of the SRC, can change continuously. The lens is assumed to provide the right amount of phase front correction on the beam to match the choice of the SRM geometry.

The difference between the broadband and the narrow band designs are all in the choice of the SRM transmissivity and the SRC tuning, as we mentioned in Sec. I. The complex optical sideband resonant frequency in the coupled SRC and AC two-cavity system is given by [16]:

$$\tilde{\omega} = \frac{ic}{2L}\log\frac{r_i + r_p e^{2i\phi_{sc}}}{1 + r_i r_p e^{2i\phi_{sc}}} \equiv -\lambda - i\epsilon \tag{16}$$

where λ and ϵ are positive and are the resonant frequency and the decay time. With our choice of signal-recycling parameters above, we get resonant sideband frequencies $\lambda = 228Hz$ and $\lambda = 1005Hz$ (The actual resonant frequency is $\omega_0 - \lambda$, i.e. the down-converted signal sideband). The PRM transmissivity and the PRC tuning are chosen such that the PRM is impedance matched to the AC and the carrier power in the AC is optimized.

The only control we do during the simulation when the mirrors are slightly deformed is to optimize the carrier power in the AC by adjust the tuning of the PRC and the AC. When optimizing the carrier power in the AC, instead of modeling the correct control signal, we look directly at the power at each equilibrium state, i.e. we do the static pseudo-control and don't model the evolution of the interferometer during the control process. With our choice of interferometer parameters given above, and a 125W input laser light power, the carrier light power in

an ideal interferometer is ~ 825kW, the power recycling rate is ~ 18 and the carrier light goes toward the dark port is ~ 0.5W.

Since our goal is to study the tolerance of the signal sideband light on mirror deformations in the degenerate SRC, we consider in our simulation only the carrier light and the resonant signal sideband (i.e. the down-converted sideband), and omit the RF sideband and other sidebands used for control purposes, as well as the other signal sideband that doesn't resonant in the system (i.e. the up-converted sideband).

After setting up the ideal interferometer, we introduce perturbations to the mirrors. We don't model the thermal effect, and assume all tilt and mis-alignment are cured by the control system, and consider only the mirror figure error. Because of the high computational load associated with the modal method, we limit our figure errors to simple profiles and thus generates leading order coupling between only a few optical modes (< 20). One focus of our study is the mirror curve radius error, which is the most interesting figure error we need to deal with, since it can be generated effectively by thermal lensing of the ITMs. To avoid the complications from the beamsplitter, we assume that it is always perfect.

At the output, we assume a mode cleaner that filtered out all HOMs in the carrier and signal sideband. So the shot noise is proportional to the square root of the output carrier power in the fundamental mode (i.e. (0,0) Gaussian mode)

$$N_{\rm shot} \propto \sqrt{I^C_{00}} \tag{17}$$

where the superscript "C" stands for carrier, and the subscript labels the mode. The signal power comes from beating the signal sideband with the carrier, both taking only the fundamental mode, so

$$S \propto \sqrt{I^C_{00}}\sqrt{I^S_{00}} \tag{18}$$

where the superscript "S" stands for signal sideband. Assuming shot noise dominating, we have

$$SNR \propto \sqrt{I^S_{00}} \tag{19}$$

i.e. the SNR is directly proportional to the signal sideband amplitude in the fundamental mode. When we take into account also the radiation pressure noise at low frequency, the change of the SNR becomes more delicate. The radiation pressure noise is omitted in this simplified model, and will be studied in a follow up detail simulation.

In the interferometer model set above, we calculate the signal sideband in two steps. In the first step, we propagate the input carrier light (Nd:YAG laser) with frequency $f_0 = 2.82 \times 10^{14}$ through the interferometer to build up the static carrier light field. In the second step, we assume a sinusoid gravitational wave of frequency f_g propagating perpendicular to the detector plane with only "+" polarization, i.e. effectively, it differentially shakes the ETMs sinusoidally with frequency f_g. In the leading order of the GW strain, two signal sidebands of frequencies $f_0 \pm f_g$ are generated at the ETMs with exactly the same mode structures as the carrier field at the ETMs. We then propagate the down-converted sideband that is tuned to be resonant in the ideal interferometer through the interferometer to build up the static signal sideband field. Repeat the second step with various GW frequencies, we can map out the frequency response of the detector. Repeat both steps with various SRC geometries and degeneracy levels, we can study the effect of the recycling cavity degeneracy on the change of frequency response and noise spectrum of the interferometer, due to mirror deformations.

The EM filed in the interferometer, which is a system of coupled optical cavities, can be written generally as

$$E = E_{\rm pump} + P_{\rm r.t.}E \tag{20}$$

where $E_{\rm pump}$ is the pumping field that contributes directly to the E field, and $P_{\rm r.t.}$ is the round trip propagator which consists free propagation operators and interaction operators that describe the propagation of E through the interferometer and back to itself. The specific form of $E_{\rm pump}$ and $P_{\rm r.t.}$ depend on the position of the E field in the interferometer. For example, for field $E_{\rm cir1}$ in Fig. 1, i.e. the circulating field in the online AC at the ITM going toward the ETM, can be written as

$$E_{\rm cir1} = t_{\rm i}T_{\rm i1}E_{\rm in1} + r_{\rm i}r_{\rm e}M_{\rm i1}P_{\rm ac1}M_{\rm e1}P_{\rm ac1}E_{\rm cir1} \tag{21}$$

where e.g. $M_{\rm i1}$ and $T_{\rm i1}$ are reflection and transmission operators of the online ITM, and we use subscript "1" and "2" to denote the online and offline cavities. We can write out a set of coupled equations in the form of Eq. (20) for all fields labeled in Fig. 1, and solve them numerically by iteration, as was done in the FFT simulation code for optical fields in LIGO [17]. In principle, we can also solve each field in terms of the input field $E_{\rm in0}$ by directly taking the inverse of all operators in the form of $(I - P_{\rm r.t.})$ (I is the identity matirx). In the FFT code, hundreds of modes are included, and it is computationally difficult to take the inverse of all the large matrices, which are sometimes nearly singular. In our simulation however, as we consider only a few (< 20) modes, we find it more efficient to take directly the matrix inversions than to iterate the fields.

In Appendix. A, we write out and solve explicitly all the carrier and signal sideband fields.

IV. SUMMARY OF SIMULATION RESULTS

Based on the optical field simulation of the simplified AdvLIGO model set up in Sec. III, we try to answer the following questions in Sec. IV A:

(i) How severe is the mode mixing in the signal sideband due to mirrors deformations, when the SRC is de-

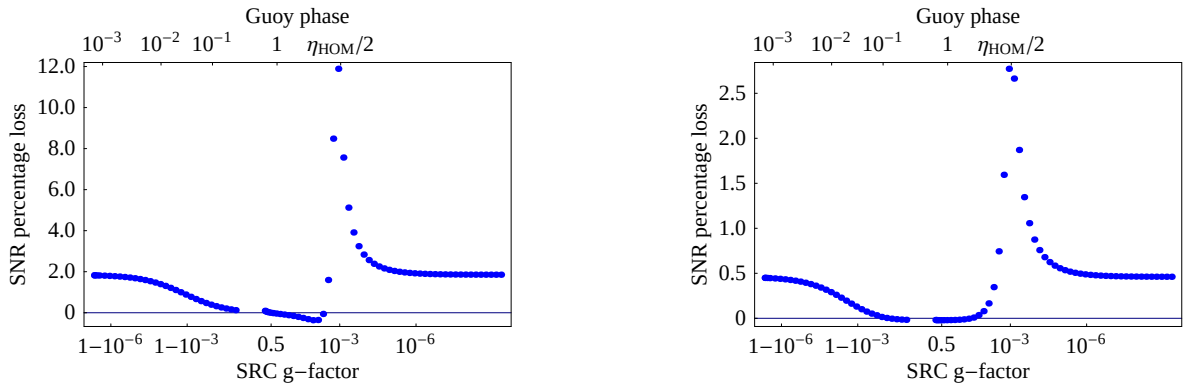

FIG. 2: SNR loss in AdvLIGO interferometers with common (left panel) and differential (right panel) curvature radius errors on the ITMs, when SRCs with various degeneracy levels are used. The SRC degeneracy level is labeled by the cavity g-factor and the one way Guoy phase.

generate? If it is severe, whether a non-degenerate SRC is able to suppress this mode mixing?

(ii) How is the carrier light affected by the SRC degeneracy level?

(iii) If a non-degenerate SRC is used, will it strongly reject the carrier or signal light coming from the AC with a mode mismatched to the eigenmodes of the SRC, and would this affect the power buildup of either the carrier or the signal light?

(iv) For broadband and narrow band AdvLIGO configurations, how different are the answers to the questions above?

(iv) Based on the answers to the questions above, what is the optimal SRC degeneracy.

In Sec. IV B, we investigate alternative designs of SRC to achieve the optimal degeneracy that might be practical in AdvLIGO.

A. Mirror figure error and optimal degeneracy

We consider mostly mirror curvature radius errors in our simulation, since they are the most likely dominant perturbations presented in the AdvLIGO due to mirror figure error or thermal lensing, and it is the lowest order perturbation on Hermite-Gaussian modes after mirror tilts having been suppressed by the control system. At the leading order, we need to consider only the (2,0) and (0,2) Hermite-Gaussian modes if there is only curvature radius error.

First, we consider a broadband interferometer with curvature radius errors on the ITMs to simulate the thermal lensing effect, and assume all other mirrors are perfect. The curvature radii of the ITMs ($R_{\rm ITM} = 2076.4m$) are changed by $\Delta R_{\rm ITM} = 5m$, either commonly or differentially, and we show the signal sideband power loss at the dark port in Fig. 2. With the change of the SRC degeneracy, characterized in the plot by the Guoy phase and the SRC g-factor, we do see significant change in the loss of the signal amplitude in the fundamental mode. In the current degenerate design, for common and differential perturbations, we lose 2% and 0.5% the signal amplitudes, or equivalently SNRs (according to Eq. (19)). Note that the leading order SNR loss in the fundamental mode is proportional to the square of the size of the error, we have, for instance, 4 times the SNR loss when ΔRITM $= 10m$. This result is also consistent with the estimation based on geometric optics approximation in Ref. [12]. When the degeneracy is reduced, the SNR loss drops by more than two orders of magnitude, and the curvature error is harmless on this aspect. More over, the most catching feature in the plots are the peaks corresponding to huge SNR loss at some non-degenerate SRC configuration. This happens when the Guoy phase of the HOMs (in this case, (2,0) and (0,2) Hermite-Gaussian modes) cancels the SRC detuning ($\phi^{\rm B}_{\rm src} = 0.06$ for broadband design), so that the HOMs of both the carrier and the signal light are resonant in the SRC while the fundamental modes are detuned. This is clearly a bad choice of SRC degeneracy, and we refer to it as the HOM resonant peak. When more HOMs are coupled into the interferometer by perturbations, we should avoid all such cavity configurations in which some HOMs have Guoy phases $\eta_{\rm HOM}$ canceling the SRC tuning phase exactly.

The effect of the SRC degeneracy on the carrier light is shown in Fig. 3, with differential curvature errors on the ITMs. Besides the HOMs resonant peaks we discussed above, there are other noticeable features about the carrier light. In the AC, curvature error harms the carrier power build-up in the way described below. When the SRC becomes non-degenerate, for common and differential curvature errors on the ITMs, both carrier and signal sideband lights behave very differently.

With common curvature error, the HOMs are coupled into the symmetric port of the interferometer, accepted by the degenerate PRC but anti-resonant in it, and get reflected back into the AC. Since the HOMs don't see the SRC, its degeneracy causes no difference. In this

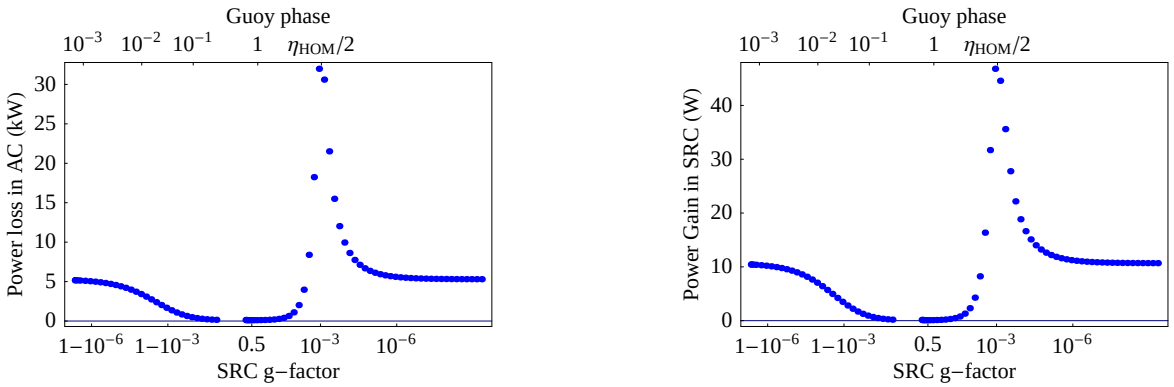

FIG. 3: Carrier light power change in the AC and SRC in AdvLIGO interferometers with differential curvature errors in the ITMs, when SRCs with various degeneracy levels are used. The SRC degeneracy level is labeled by the cavity g-factor and the one way Guoy phase.

case the carrier light power is controlled by the AC and is hardly affected by the mirror deformations, thus we didn't show it. The SNR loss in this case is due directly to the coupling of signal light HOMs to the dark port.

With differential curvature error, however, the HOMs are coupled to antisymmetric port of the interferometer, and and when the SRC is degenerate, since the carrier light is not anti-resonant in it, it behaves like "resonant carrier extraction", and sucks carrier light out of the AC thus reduces its power buildup. When SRC is non-degenerate, HOMs are rejected by both the SRC and the AC, and the carrier power builds up as usual in the AC in almost entirely its fundamental mode without losing any significant power. The SNR loss in this case is due directly to the loss of carrier power in the AC, since the signal light HOMs are coupled to the symmetric port and are rejected by the PRC which is not detuned for the signal sideband frequency.

In conclusion, common and differential errors in the ACs reduce the SNR through different ways and the differential errors reduce the carrier buildup significantly. Finally, as indicated above by "resonant carrier extraction", the differential curvature errors send a huge amount of carrier power in HOMs toward the dark port (10W in HOMs and 0.3W in fundamental modes inside the SRC), and thus sends a reference light that is mostly in the HOMs toward the photon detector, which must be cleaned out by the output mode cleaner.

Now we turn to the third question in the beginning of Sec. IV. To answer it, we consider ACs and SRC with different curvature error or even different mode of perturbations. In Fig. 4, we show the SNR loss for various SRC degeneracy levels, when there are common curvature radius errors of $\Delta R = 5$m on the ITMs and different curvature radius error and several 4^{th} order figure errors (i.e. distortion function $Z(x, y)$ is a linear combination of $H_4(x)H_0(y)$, $H_0(x)H_4(y)$, and $H_2(x)H_2(y)$) of comparable sizes on the SRM. Comparing with Fig. 2, we see more SNR loss with degenerate SRC due to the

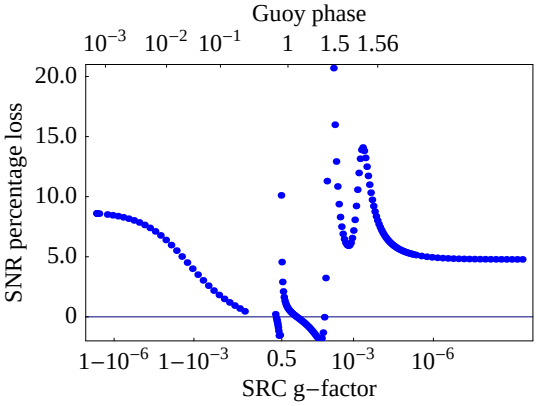

FIG. 4: SNR loss in AdvLIGO interferometers with common curvature radius errors on the ITMs and curvature error and 4^{th} order Hermite polynomial shaped figure error on the SRM, when SRCs with various degeneracy levels are used. The SRC degeneracy level is labeled by the cavity g-factor and the one way Guoy phase.

excitation of more HOMs, i.e. the 4^{th} order Hermite-Gaussian modes, and we see two more HOM resonant peaks generated by the 4^{th} order modes. We can see from Fig. 4 that, although the optical modes in the AC and the SRC are different, and there is an eigenmode mismatching on the ITMs, the non-degenerate SRC doesn't simply reject part of the signal power, and the SNR loss is still very low (away from those HOM resonant peaks). This is because the SRC effectively filters out the HOMs that cause the mode mismatch and helps the fundamental mode buildup in the AC, as long as the SRC tuning for the signal sideband fundamental mode resonance is unchanged (this depends on how the control system works, and the modeling of control sidebands are being considered in the more sophisticated simulations under development, e.g. the AdvLIGO FFT simulation [18]).

All examples above are simulations with broadband

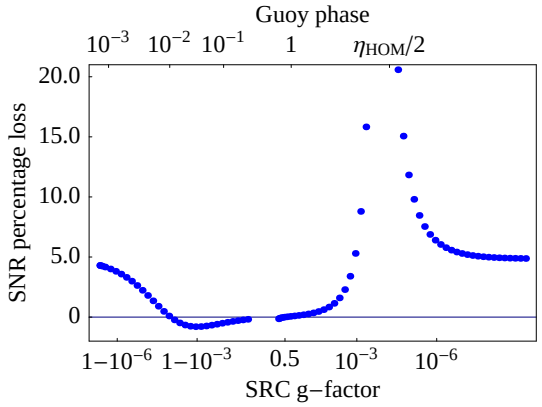

FIG. 5: SNR loss in an advanced narrowband interferometer with common curvature radius errors on the ITMs, when SRCs with various degeneracy levels are used. The SRC degeneracy level is labeled by the cavity g-factor and the one way Guoy phase.

AdvLIGO configuration, i.e. under the RSE scheme, in which signal storage time is reduced by the SRC. In the narrowband configuration, however, the signal light is indeed being "recycled", and the storage time in the SRC is order of magnitude longer than in the RSE scheme, which could change our results for broadband interferometer significantly. In Fig. 5, we show the result of a narrowband configuration with differential curvature errors $\Delta R = 2m$ on the ITMs. Again, we got similar result as before, i.e. SNR loss is suppressed by non-degenerate SRC by order of magnitude. The loss in degenerate SRC is about 5%, which is significant. In Ref. [12], the most severe constraint on mirror figure error is also placed on the narrowband configuration. The SRC finesse in the narrow-band configuration is much higher than the broad-band AdvLIGO configuration, so that the HOMs being excited inside the SRC is built up to higher power, when the SRC is degenerate.

From the examples above, we can see that the mode mixing and the consequent problems are suppressed with non-degenerate SRC, and the optimal Guoy phase in the SRC for Hermite-Gaussian mode should be somewhere between 0.25 and 1 radian, with best range between 0.4 and 0.7 radian. In the examples above we showed only at the most sensitive signal sideband frequency (given by Eq. (16)) that the signal power or SNR loss is suppressed by non-degenerate SRC. In Fig. 6, we show the interferometer response to various signal frequencies assuming that the SRC is either degenerate with current design parameters or non-degenerate with the MMT design suggested by Müller [10]. There is indeed an strong suppression of the SNR loss across the entire AdvLIGO sensitive band, with some shift of the most sensitive frequency (remember however that at low frequency ($< 100Hz$), we need to consider also the radiation pressure noise).

At first sight, there seems to be a wide range for us to choose the SRC degeneracy, but our freedom is actually quite limited. One obvious constraint is that we need to avoid those Guoy phases giving rise to the HOM resonant peaks. In a realistic interferometer, with many more HOM perturbations, there would be a huge number of HOM resonant peaks across the optimal Guoy phase range so the degeneracy should be chosen carefully, through careful simulations.

However, the worst difficulty posed by the above Guoy phase range is a practical one. There are two obvious ways to achieve this g-factor by changing the SRC design: reduce the beam size, or increase the cavity length. Unfortunately, to achieve the low degeneracy required above, we need either very small beam waist size near the SRM, or kilometer-long recycling cavity length. In the next section, we discuss the practical alternative designs to reduce the SRC degeneracy to the optimal range.

B. Alternative designs

There are basically two ways to reduce the SRC degeneracy: either reduce the beam size or increase the cavity length. We discuss both ideas respectively in the following.

To reduce the beam size in the SRC we could add a lens in the recycling cavity, but to get the Guoy phase range between 0.25 and 1 radian, the beam should be so strongly focused that the beam waist size is on the order of $30\mu m$, and the waist should also be tuned precisely several millimeters away from the SRM. If we have $10\mu m$ scale beam size on the SRM, we are looking at an unpractical $10GW/m^2$ power density. This problem is pointed out qualitatively by Bochner [17] in his FFT simulation work.

We can bypass this problem by introducing multiple steps of beam focusing, i.e. bring down the beam size step by step with more optical elements, such that there is some Guoy phase accumulated during each step with relatively small beam size, and clearly that we prefer reflective optical elements in this scheme than lens. A practical design of moving the mode matching telescope (MMT) into the recycling cavity is proposed by Müller [10], in which the MMTs outside the recycling cavities used to match the beam size between the laser source and the PRM, and the SRM and the photon detector are moved into the cavities to reduce the beam size. Two mirror are used in each MMT, where the first brings down the beam size from $\sim 6cm$ to millimeter scale, and the second tune the shape of the millimeter scale beam to achieve the desired degeneracy. The MMT introduces more mirrors and cavities into the interferometer, so there are concerns about the stability of the cavities and the control of the new mirrors. Practical parameters for the PRC can be found in Ref. [10], and the coupled recycling cavities and cavities in the MMT are stable in principle. Experimental work on issues about implementing this MMT design is under going.

Another way to reduce the SRC degeneracy is to use

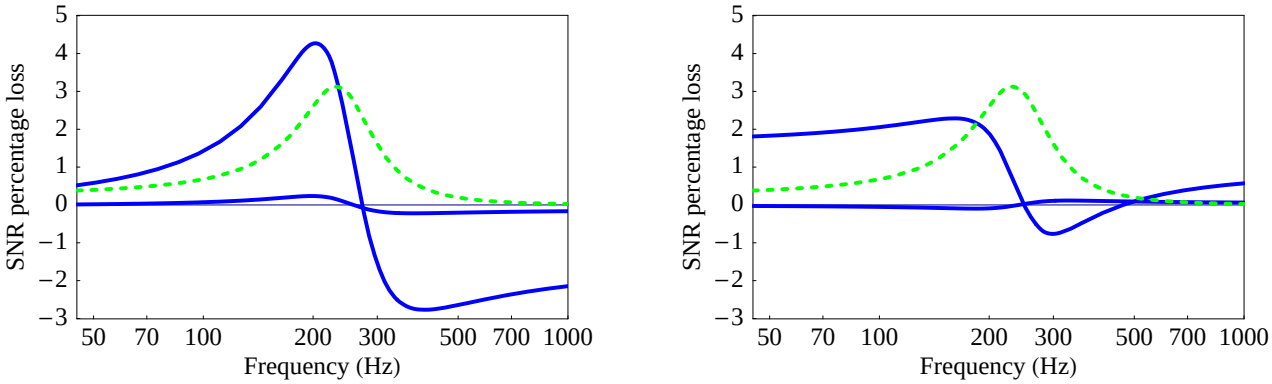

FIG. 6: SNR loss in AdvLIGO interferometers with common (left panel) and differential (right panel) curvature radius errors on the ITMs, for signal with various frequnecies. In each plot, the solid curve with larger variation is the SNR loss when the SRC is degenerate; the other solid curve is the SNR loss when the SRC is non-degenerate at the level given by the MMT design (with one way cavity Guoy phase ~ 0.38); the dashed curve is the frequency response function of the ideal AdvLIGO interferometer, plotted in arbitrary unit for reference.

longer SRC, while the length must be kilometer-long before making any difference. A natural idea is to bend the SRC into the arm cavity tubes and make it $4km$ long. This design is much more radical, and has the immediate problem of light scattering noise in the crowded arm tubes, but it does have important scientific advantages. The $4km$ SRC design has been suggested for a long while, and reducing the SRC degeneracy is really just a "gift" here among other advantages expected from long recycling cavity. Mizuno [5] suggested to use a $4km$ long SRC to collect power in both signal sidebands and increase the SNR by a factor of $\sqrt{2}$. Buonanno and Chen, among their discussion on beating the SQL with signal recycled interferometer, found also that the gain in peak sensitivity is vulnerable to optical loss in the short SRC, while long SRC might solve this problem. Moreover, long SRC introduce frequency dependent correlation between the two quadratures of the vacuum field, and might bring interesting change to the optical noise spectrum of the interferometer.

V. CONCLUSIONS

We set up a simplified AdvLIGO interferometer model with perturbations on the mirrors in the form of figure errors, and simulated the carrier and signal sideband optical fields in the interferometer through a mode decomposition approach. Using the simulation result, we investigated the loss of SNR and carrier power with SRCs at various degeneracy levels, and proposed the optimal SRC degeneracy level to suppress these losses.

With the current degenerate SRC design, we found the SNR loss due to mode mixing between the fundamental mode and HOMs significant, and the result is consistent with the order of magnitude estimation in Ref. [12]. We found a 2% loss in SNR, with $5m$ curvature radius error on the ITMs, or even smaller mirror figure error on the SRM. If we consider the perturbation in terms of figure error, these curvature errors correspond to roughly $5nm$ peak-to-valley figure error in the center region of the mirror. Consider the fact that at leading order, this loss grows quadratically with the size of the figure errors, and losses due to errors with different Hermite polynomial modes are added linearly, the constraint on mirror figure errors and thermal effects is quite severe. Another problem we found with degenerate SRC is that, when there are differential perturbations on the ACs, huge amount of HOMs power is coupled to the dark port and overwhelms the reference light in fundamental mode, which requires a reliable output mode cleaner.

We showed then that non-degenerate SRC could solve the problems above, suppress the mode mixing and reduce the SNR loss by orders of magnitude, for signals with frequencies in the AdvLIGO sensitive band. We showed also that the non-degenerate SRC would not simply reject laser light from the AC with mode mismatch, but rather filter out the HOMs and help the fundamental mode buildup.

Based on the facts above, we proposed to use non-degenerate SRC in the AdvLIGO with optimal Guoy phase between 0.25 and 1 radian. This optimal level of degeneracy is, however, hard to achieve in practice, and we discussed some possible alternative designs of the SRC to reduce the degeneracy to the optimal level, including moving the MMT into the recycling cavities and using a $4km$ long SRC.

A more complete simulation of the optical field inside the AdvLIGO interferometer using FFT propagation scheme is under development [18], which will effectively include hundreds of HOMs, and the modeling of important physical factors like the thermal effect on the mirrors, and other control sideband fields. This new simulation is aimed at mapping out the phase front of light

fields in a very realistic model of the AdvLIGO interferometer to the very high accuracy level of 10^{-6}, and among other goals helping design SRC with optimal degeneracy.

Acknowledgments

I wish to thank K. Thorne for suggesting this problem. I thank Guido Müller, Phil Willems, Kip Thorne and Hiroaki Yamamote for very useful discussions and interactions.

APPENDIX A: SOLVE THE OPTICAL FIELDS IN THE INTERFEROMETER

In this appendix, I will write out the equations in the form of Eq. (20) for all carrier and signal sideband fields displayed in Fig. 1 and solve them analytically in terms of the input field $E_{\rm in0}$, the GW strain, and the propagation and interaction operators in the interferometer.

The carrier light and the signal light have inputs from different positions (the signal input is effectively at the ETMs), their solutions are different and have to be treated separately. I will in the following denote with superscripts "C" for carrier and "S" for signal. Furthermore, because of their different frequency, their propagation operators have to be distinguished as well in the AC, while for the short recycling cavities, since the fractional difference between the frequencies is on the order of 10^{-11}, the phase difference between carrier and signal lights are negligible and we use the same operators. For the same reason, interaction operators are the same for carrier and signal light, in which the perturbation effect has effectively a length scale $\sim$ 10nm.

As described in Sec. III, we solve as the first step the carrier field. Using results for LIGO that has been derived in Ref. [14] and Ref. [19], following the convention in Sec. III, we define:

Round-trip propagator in the AC

$$\begin{aligned} P^{\rm C}_{\rm rtac1} &= r_{\rm i1}r_{\rm e1}M_{\rm i1}P^{\rm C}_{\rm ac1}M_{\rm e1}P^{\rm C}_{\rm ac1} \\ P^{\rm C}_{\rm rtac2} &= r_{\rm i2}r_{\rm e2}M_{\rm i2}P^{\rm C}_{\rm ac2}M_{\rm e2}P^{\rm C}_{\rm ac2} \end{aligned} \tag{A1}$$

again we use subscript "1" and "2" to denote online of offline arm cavities;

Reflection operator of the ACs (for reflecting off the AC from the ITM side)

$$\begin{aligned} M^{\rm C}_{\rm ac1} &= r_{\rm i1}\left(M'_{\rm i1} - \frac{t^2_{\rm i1}}{r^2_{\rm i1}}T_{\rm i1}M^{\dagger}_{\rm i1}P^{\rm C}_{\rm rtac1}(I-P^{\rm C}_{\rm rtac1})^{-1}T_{\rm i1}\right) \\ M^{\rm C}_{\rm ac2} &= r_{\rm i2}\left(M'_{\rm i2} - \frac{t^2_{\rm i2}}{r^2_{\rm i2}}T_{\rm i2}M^{\dagger}_{\rm i2}P^{\rm C}_{\rm rtac2}(I-P^{\rm C}_{\rm rtac2})^{-1}T_{\rm i2}\right) \end{aligned} \tag{A2}$$

where $M'_{\rm i1}$ and $M'_{\rm i2}$ are reflection operators of the ITMs seen from the recycling cavity side;

Michelson operators

$$\begin{aligned} M^{\rm C}_{\rm C} &= t^2_{\rm p}P^{\rm C}_{\rm d}M^{\rm C}_{\rm ac1}P^{\rm C}_{\rm d} + r^2_{\rm p}P^{\rm C}_{\rm -d}M^{\rm C}_{\rm ac2}P^{\rm C}_{\rm -d} \\ M^{\rm C}_{\rm D} &= t_{\rm p}r_{\rm p}(P^{\rm C}_{\rm d}M^{\rm C}_{\rm ac1}P^{\rm C}_{\rm d} + P^{\rm C}_{\rm -d}M^{\rm C}_{\rm ac2}P^{\rm C}_{\rm -d}) \end{aligned} \tag{A3}$$

where $P^{\rm C}_{\rm d}$ and $P^{\rm C}_{\rm -d}$ are propagators through the length difference d of the Michelson arms.

The coupled equations for the carrier fields are then:

$$\begin{aligned} E^{\rm C}_{\rm s} &= t_{\rm bs}P^{\rm C}_{\rm prc}P^{\rm C}_{\rm d}E^{\rm C}_{\rm re1} - r_{\rm bs}P^{\rm C}_{\rm prc}P^{\rm C}_{\rm -d}E^{\rm C}_{\rm re2} \\ E^{\rm C}_{\rm a} &= r_{\rm bs}P^{\rm C}_{\rm src}P^{\rm C}_{\rm d}E^{\rm C}_{\rm re1} + t_{\rm bs}P^{\rm C}_{\rm src}P^{\rm C}_{\rm -d}E^{\rm C}_{\rm re2} \\ E^{\rm C}_{\rm sr} &= -r_{\rm p}M_{\rm p}E^{\rm C}_{\rm s} + t_{\rm p}E_{\rm in0} \\ E^{\rm C}_{\rm ar} &= -r_{\rm s}M_{\rm s}E^{\rm C}_{\rm a} \\ E^{\rm C}_{\rm in1} &= t_{\rm bs}P^{\rm C}_{\rm prc}P^{\rm C}_{\rm d}E^{\rm C}_{\rm sr} + r_{\rm bs}P^{\rm C}_{\rm src}P^{\rm C}_{\rm d}E^{\rm C}_{\rm ar} \\ E^{\rm C}_{\rm in2} &= -r_{\rm bs}P^{\rm C}_{\rm prc}P^{\rm C}_{\rm -d}E^{\rm C}_{\rm sr} + t_{\rm bs}P^{\rm C}_{\rm src}P^{\rm C}_{\rm -d}E^{\rm C}_{\rm ar} \\ E^{\rm C}_{\rm re1} &= M^{\rm C}_{\rm ac1}E^{\rm C}_{\rm in1} \\ E^{\rm C}_{\rm re2} &= M^{\rm C}_{\rm ac2}E^{\rm C}_{\rm in2} \end{aligned} \tag{A4}$$

and the circulating fields inside the AC are given in terms of $E^{\rm C}_{\rm in1}$ and $E^{\rm C}_{\rm in2}$:

$$\begin{aligned} E^{\rm C}_{\rm cir1} &= t_{\rm i1}P^{\rm C}_{\rm ac1}\left(I-P^{\rm C}_{\rm rtac1}\right)^{-1}T_{\rm i1}E^{\rm C}_{\rm in1} \\ E^{\rm C}_{\rm cir2} &= t_{\rm i2}P^{\rm C}_{\rm ac2}\left(I-P^{\rm C}_{\rm rtac2}\right)^{-1}T_{\rm i2}E^{\rm C}_{\rm in2} \end{aligned} \tag{A5}$$

Solving Eq. (A4), we have:

$$\begin{aligned} E^{\rm C}_{\rm sr} &= t_{\rm p}\Big(I + r_{\rm p}M_{\rm p}P^{\rm C}_{\rm prc}M^{\rm C}_{\rm C}P^{\rm C}_{\rm prc} - r_{\rm p}r_{\rm s}M_{\rm p}P^{\rm C}_{\rm prc}M^{\rm C}_{\rm D}P^{\rm C}_{\rm src} \\ &\quad \times \left(I + r_{\rm s}M_{\rm s}P^{\rm C}_{\rm src}M^{\rm C}_{\rm C}P^{\rm C}_{\rm src}\right)^{-1}M_{\rm s}P^{\rm C}_{\rm src}M^{\rm C}_{\rm D}P^{\rm C}_{\rm prc}\Big)^{-1}E_{\rm in0} \\ E^{\rm C}_{\rm ar} &= -\left(I + r_{\rm s}M_{\rm s}P^{\rm C}_{\rm src}M^{\rm C}_{\rm C}P^{\rm C}_{\rm src}\right)^{-1}r_{\rm s}M_{\rm s}P^{\rm C}_{\rm src}M^{\rm C}_{\rm D}P^{\rm C}_{\rm prc}E^{\rm C}_{\rm sr} \end{aligned} \tag{A6}$$

All other carrier fields can be easily calculated from $E^{\rm C}_{\rm sr}$ and $E^{\rm C}_{\rm ar}$.

Assuming a monochromatic GW wave passing through the interferometer shaking the ETMS differentially with strain $h_0\cos\omega_g t$, the carrier light that is incident on the ETMs (i.e. $E^{\rm C}_{\rm cir1}$ and $E^{\rm C}_{\rm cir2}$) are coupled to the motion of the ETMs and generates signal sidebands at frequencies $\omega \pm \omega_g$ with the EM fields given by

$$\begin{aligned} E^{\rm S}_{\rm sig1} &= i\phi_h r_{\rm e1}M_{\rm e1}E^{\rm C}_{\rm cir1} \\ E^{\rm S}_{\rm sig2} &= -i\phi_h r_{\rm e2}M_{\rm e2}E^{\rm C}_{\rm cir2} \end{aligned} \tag{A7}$$

where $\phi_h = 2kh_0L$ is the phase shift due to the GW strain. These fields are the input for the signal light field in the interferometer.

For signal sideband field, we define round-trip propagator of the AC:

$$\begin{aligned} P^{\rm S}_{\rm rtac1} &= r_{\rm i1}r_{\rm e1}M_{\rm e1}P^{\rm C}_{\rm ac1}M_{\rm i1}P^{\rm C}_{\rm ac1} \\ P^{\rm S}_{\rm rtac2} &= r_{\rm i2}r_{\rm e2}M_{\rm e2}P^{\rm C}_{\rm ac2}M_{\rm i2}P^{\rm C}_{\rm ac2} \end{aligned} \tag{A8}$$

and we define the Michelson operators the same way as in Eq. (A3)

The coupled equations for the signal fields are similar to Eq. (A4), and we only need to change all quantities for the carrier fields in Eq. (A4) to their counterparts for the signal fields, and change the positions of the input fields in three of the equations given below

$$\begin{aligned} E^{\rm S}_{\rm sr} &= -r_{\rm p} M_{\rm p} E^{\rm S}_{\rm s} \\ E^{\rm S}_{\rm re1} &= M^{\rm S}_{\rm ac1} E^{\rm S}_{\rm in1} + t_{\rm i1} T_{\rm i1} P^{\rm S}_{\rm ac1} \left(I - P^{\rm S}_{\rm rtac1}\right)^{-1} E^{\rm S}_{\rm sig1} \\ E^{\rm S}_{\rm re2} &= M^{\rm S}_{\rm ac2} E^{\rm S}_{\rm in2} + t_{\rm i2} T_{\rm i2} P^{\rm S}_{\rm ac2} \left(I - P^{\rm S}_{\rm rtac2}\right)^{-1} E^{\rm S}_{\rm sig2} \end{aligned} \tag{A9}$$

Solving Eq. (A9), we have the output signal field:

$$\begin{aligned} E^{\rm S}_{\rm out} &= t_{\rm s} \left(I + r_{\rm s} P^{\rm S}_{\rm src} M^{\rm S}_{\rm C} P^{\rm S}_{\rm src} M_{\rm s}\right)^{-1} \\ &\quad \times \left(-r_{\rm p} P^{\rm S}_{\rm src} M^{\rm S}_{\rm D} P^{\rm S}_{\rm prc} M_{\rm p} E^{\rm S}_{\rm s} + E^{\rm S}_{\rm siga}\right) \end{aligned} \tag{A10}$$

where

$$\begin{aligned} E^{\rm S}_{\rm s} &= \Big(I + r_{\rm p} P^{\rm S}_{\rm prc} M^{\rm S}_{\rm C} P^{\rm S}_{\rm prc} M_{\rm p} - r_{\rm p} r_{\rm s} P^{\rm S}_{\rm prc} M^{\rm S}_{\rm D} P^{\rm S}_{\rm src} M_{\rm s} \\ &\quad \left(I + r_{\rm s} P^{\rm S}_{\rm src} M^{\rm S}_{\rm C} P^{\rm S}_{\rm src} M_{\rm s}\right)^{-1} P^{\rm S}_{\rm src} M^{\rm S}_{\rm D} P^{\rm S}_{\rm prc} M_{\rm p}\Big)^{-1} \\ &\quad \times \Big(E^{\rm S}_{\rm sigs} - r_{\rm s} P^{\rm S}_{\rm prc} M^{\rm S}_{\rm D} P^{\rm S}_{\rm src} M_{\rm s} \\ &\qquad \times \left(I + r_{\rm s} P^{\rm S}_{\rm src} M^{\rm S}_{\rm C} P^{\rm S}_{\rm src} M_{\rm s}\right)^{-1} E^{\rm S}_{\rm siga}\Big) \\ E^{\rm S}_{\rm sigs} &= t_{\rm i1} t_{\rm bs} P^{\rm S}_{\rm prc} P^{\rm S}_{\rm d} T_{\rm i1} P^{\rm S}_{\rm ac1} \left(I - P^{\rm S}_{\rm rtac1}\right)^{-1} E^{\rm S}_{\rm sig1} \\ &\quad - t_{\rm i2} r_{\rm bs} P^{\rm S}_{\rm prc} P^{\rm S}_{-\rm d} T_{\rm i2} P^{\rm S}_{\rm ac2} \left(I - P^{\rm S}_{\rm rtac2}\right)^{-1} E^{\rm S}_{\rm sig2} \\ E^{\rm S}_{\rm siga} &= t_{\rm i1} r_{\rm bs} P^{\rm S}_{\rm src} P^{\rm S}_{\rm d} T_{\rm i1} P^{\rm S}_{\rm ac1} \left(I - P^{\rm S}_{\rm rtac1}\right)^{-1} E^{\rm S}_{\rm sig1} \\ &\quad + t_{\rm i2} t_{\rm bs} P^{\rm S}_{\rm src} P^{\rm S}_{-\rm d} T_{\rm i2} P^{\rm S}_{\rm ac2} \left(I - P^{\rm S}_{\rm rtac2}\right)^{-1} E^{\rm S}_{\rm sig2} \end{aligned} \tag{A11}$$

[1] P. Fritshel, Proc. SPIE **4856-39**, 282 (2002)

[2] See, *e.g.*, LIGO Scientific Collaboration, Phys. Rev. D **69**, 082004 (2004); **69**, 102001 (2004); **69**, 122001 (2004); **69**, 122004 (2004).

[3] J. Y. Vinet, B. Meers, C. N. Man, and A. Brillet, Phys. Rev. D **38**, 433 (1988); B. J. Meers, *ibid.* 2317 (1988).

[4] J. Mizuno, K. A. Strain, P. G. Nelson, J. M. Chen, R. Schilling, A. Rüdiger, W. Winkler, and K. Danzmann, Phys. Lett. A **175**, 273 (1993).

[5] J. Mizuno, Ph.D. thesis, Max-Planck-Institut für Quantenoptik, Garching, 1995.

[6] G. Heinzel, Ph.D. thesis, Max-Planck-Institut für Quantenoptik, Garching, 1999.

[7] K. S. Thorne, "The scientific case for mature LIGO interferometers" LIGO Document Number P000024-00-R, www.ligo.caltech.edu/docs/P/P000024-00.pdf; C. Cutler and K. S. Thorne, "An overview of gravitational-wave sources", gr-qc/0204090.

[8] J. A. Arnaud, Appl. Opt. **8**, 189-195 (1969).

[9] R. Lawrence, Ph.D. thesis, MIT, 2003.

[10] G. Müller and S. Wise, "Mode Matching in Advanced LIGO", LIGO Document Number T020026-00-D, www.ligo.caltech.edu/docs/T/T020026-00.pdf

[11] Private communication.

[12] E. D'Ambrosio, R. O'Shaughnessy, S. Strigin, K. S. Thorne and S. Vyatchanin, gr-qc/0409075, Submitted to Phys. Rev. D

[13] A. E. Siegman, *Lasers*, (University science, Mill Valley, 1986).

[14] Y. Hefetz, N. Mavalvala and D. Sigg, "Principles of Calculating Alignment Signals in Complex Resonant Optical Interferometers", LIGO Document Number P960024-A-D, www.ligo.caltech.edu/docs/P/P960024-A.pdf

[15] J. Vinet, P. Hello, C. Man and A. Brillet, J. Phys. I France **2**, 1287 (1992).

[16] A. Buonanno and Y. Chen, Phys. Rev. D. **67**, 062002 (2003).

[17] B. Bochner, Ph.D. thesis, MIT, 1998.

[18] Y. Pan, P. Willems and H. Yamamoto, "FFT Simulation Note 1: Formulation", LIGO Document Number T050218-00-E, www.ligo.caltech.edu/docs/T/T050218-00.pdf

[19] D. Sigg, "Modal Model Update 1: Interferometer Operators", LIGO Document Number T960113-00-D, www.ligo.caltech.edu/docs/T/T960113-00.pdf